Iranian Journal of Chemical Engineering
Vol. 14, No. 2 (Spring 2017), IAChE

A Numerical Simulation Model of Solid Acid Fuel Cell Performance by CsH_2PO_4 Electrolyte

I. Omidi, M. Kalbasi*

Chemical Engineering Department, Amir Kabir University of Technology, P. O. Box: 15875-4413, Tehran, Iran

ARTICLE INFO

Article history:
Received: 2016-04-01
Accepted: 2016-09-25

Keywords:
SAFC
Fuel Cells
CsH_2PO_4 Electrolyte
Solid Acids Composite

ABSTRACT

The performance of the solid acid fuel cell by CsH_2PO_4 electrolyte was analyzed using the present model of the electrochemical reaction and transport phenomena, which are fully coupled with the governing equations. Development of such a model requires creating the three-dimensional geometry and its mesh grid, discretization of momentum, mass and electric charge balance equation and solving the equations based on the information of electrical and electrochemical models in different areas of the cell consisting of porous electrodes, gas channels, and the solid parts like the current collector. The model equations were solved employing a finite elements technique solver of cell potential. Different parameters including current density (i), cell potential (V), cell power and concentration distribution of hydrogen, oxygen and water vapor have been investigated in this study. Also, the effect of different voltages on the concentration distribution of all the mentioned species through the cell length are taken into account. The results showed that there is a noticeable difference between H_2, O_2 and H_2O concentration through the cell length subjected to various voltages. This difference was more apparent at lower voltages due to higher current density and higher consumption of species. The polarization curve is suitably consistent with the model and experimental data which verify the present simulation results.

1. Introduction

Due to their high efficiencies and low pollution levels fuel cells are becoming attractive alternatives to combustion engines for electrical power generation [1-5]. In recent years, new fuel cells based on solid acid electrolytes, such as the compounds CsH_2PO_4 and $CsHSO_4$, have resulted in higher power density and lower cost membranes [6-8].

Operating at mid-range temperatures (380 K-550 K), solid acid fuel cell stacks tolerate impurities that pose obstacles for other fuel cell technologies, using inexpensive metal components. Solid acids are used in applications as proton transport membranes while also acting as electrical insulators [9,10]. This is due to fact that proton

*Corresponding author: mkalbasi@aut.ac.ir

conduction through solid acids is several orders of magnitude higher than that of electron conduction.

CsH_2PO_4 belongs to a category of solid acid electrolytes known as MH_2XO_4 type solid acids. The M represents an atom in the alkali group, such as cesium, potassium or rubidium, while the X is an atom of the pnictogens group (5a) such as phosphorus or arsenic [11-15]. When a normal acid, such as phosphoric acid, reacts with a normal salt such as cesium phosphate, it ends up with cesium dihydrogen phosphate as shown below:

$$Cs_3PO_4 + 2H_3PO_4 \rightarrow 3CsH_2PO_4 \quad (1)$$

This particular acid has been chosen because it is relatively well characterized, low cost, high power density, flexibility in fuel choice and its superprotonic phase has a reasonably wide temperature range of stability, from the transition at 228 ˚C to dehydration at temperatures higher than 260 ˚C. In these temperatures CsH_2PO_4 dehydrates to solid $CsPO_3$ with a decrease of conductivity as shown below [16-19]:

$$CsH_2PO_4 \leftrightarrow CsPO_3 + H_2O \quad (2)$$

The high operating temperature for CsH_2PO_4 based fuel cells opens up possibilities for the direct utilization of fuel cells other than hydrogen. Because CsH_2PO_4 undergoes such a remarkable change in proton conductivity when transitioning from the lower temperature to the superprotonic phase, the mechanics of proton conduction are of interest. In the mechanism of proton conduction in CsH_2PO_4 proposed by Grotthus, a proton transfers along hydrogen bonding between two adjacent PO_4^{-3} groups (B in Fig. 1). This group rotates bringing the attached proton into proximity with a different PO_4^{-3} group (C in Fig. 1) and then proton transfer along the newly formed hydrogen bond to the next PO_4^{-3} group (D in Fig. 1) [20-22].

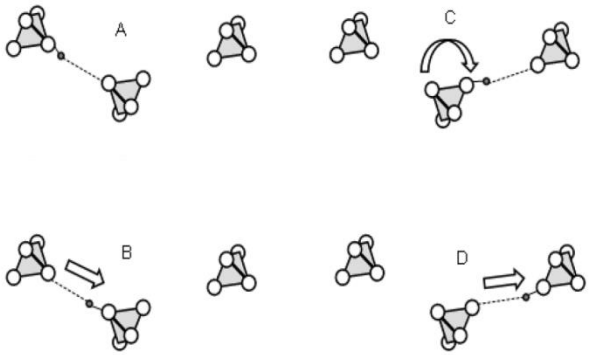

Figure 1. Grotthus mechanism of proton conducting in CsH_2PO_4.

Yang et al. [23] have reported approaches to the development of high temperature membranes for proton exchange membrane fuel cells. The viability of CsH_2PO_4 based fuel cells was first studied by the authors in [24].The feasibility of CsH_2PO_4 to be used as the electrolyte for both hydrogen and methanol fuel cells under intermediate conditions, and later the polarization measurements reported by Otomo et al. in [25] were demonstrated. Haile et al. [26] studied phase transition behavior, conductivity and configurational entropy of superprotonic CsH_2PO_4. Ponomareva et al. [27] presented a comparative study of transport and thermodynamic properties of CsH_2PO_4. Xie et al. [28] reported a composite electrolyte membrane based on CsH_2PO_4, sulfonated poly (ether ether ketone) and phosphosilicate sol. The prepared electrolyte membrane exhibits excellent mechanical performance. Qing et al. [29] prepared CsH_2PO_4/epoxy composite electrolytes by dispersing CsH_2PO_4 particles which showed a

high thermal stability with no weight loss or phase transformation up to 290 ˚C.

Despite rapid progress in solid acid fuel cells, optimization of these systems for commercial use is a great challenge for the researchers. For this purpose, mathematical models and simulation are employed as tools to design optimized fuel cells, stacks and the fuel cell power system. For example, modeling of a solid oxide fuel cell based on the transient behavior of the chemical reactions was reported in [30] and a dynamic model of a high temperature proton exchange membrane fuel cell with a fuel processor is developed in [31]. However, to the best knowledge of the authors, there are few published reports on the investigation of solid acid fuel cell by CsH_2PO_4 electrolyte in the literature.

The purpose of this study is to develop a model to predict the three-dimensional solid acid fuel cell operating parameters, such as the concentration distribution, current density and the polarization curve. We first generate the geometry and its mesh grid then we discretize and solve momentum, mass and electric balance equations simultaneously.

This model investigates the steady-state transport of reactants and water in a cell including both anode and cathode mass and momentum transport phenomena in the flow channels, gas diffusion layers (GDLs) and porous electrodes, as well as electrochemical currents in the GDLs, the porous electrodes and the electrolyte.

2. Theory

The solid acid fuel cell is comprised of two electrodes (anode and cathode) separated by a solid membrane acting as an electrolyte. Fuel flows through a network of channels toward the anode, where it dissociates into protons. Then, protons flow through the membrane toward the cathode and electrons that are collected as electrical current by an external circuit linking the two electrodes. The oxidant (air in this study) also flows through a similar network of channels to the cathode. Then electrons in the external circuit and the protons flowing through the membrane mingle with oxidant and produce water. Here, the electricity current is generated by a flow of electrons from the anode toward the cathode through the external circuit. We may utilize the number of cells in a series to make up a stack to deliver sufficient electricity.

The electrochemical reactions involved in a solid acid fuel cell are as follows:

$$H_2 \rightarrow 2H^+ + 2e^- \tag{3}$$

$$O_2 + 4H^+ + 4e^- \rightarrow 2H_2O \tag{4}$$

$$H_2 + \frac{1}{2}O_2 \rightarrow H_2O \tag{5}$$

The primary assumptions used in the development of our model are:

- Gas diffusion layers, catalyst layers and electrolyte are considered homogeneous and isotropic porous media.
- Flow is laminar and incompressible due to the low velocities and pressure gradients.
- Electrochemical reactions take place at the electrode-electrolyte boundaries.
- All gas mixtures are assumed to behave as ideal gas and the cell operates under steady-state conditions.

Figure 2 shows a schematic diagram of a typical computational domain for a solid acid fuel cell. The fuel cell is composed of two porous layers (called gas diffusion layers,

GDLs), each using a thinner electro-catalyst layer on the face to contact with the interposed electrolyte.

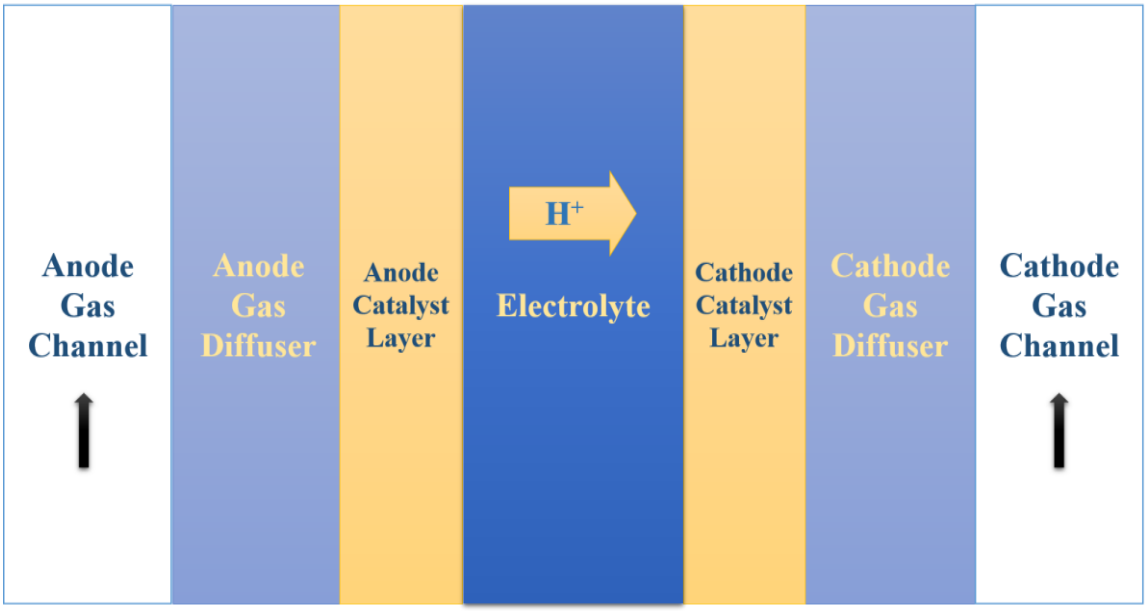

Figure 2. Schematic of solid acid fuel cell.

A three-dimensional solid acid fuel cell with co-current flow direction of air and fuel is modeled. Figure 3 shows the geometry of modeled fuel cell in detail.

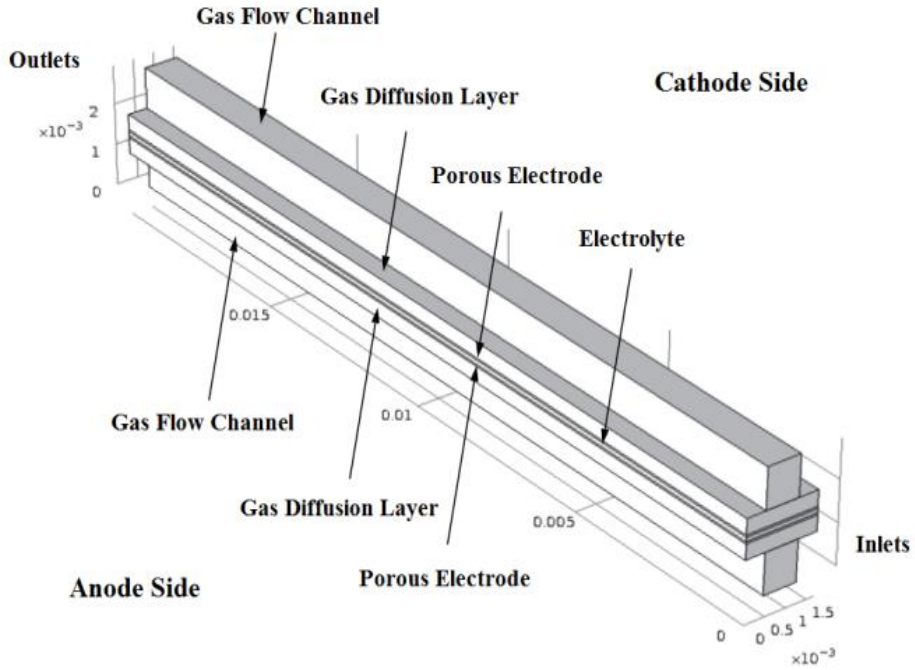

Figure 3. A 3D solid acid fuel cell model computational domain.

During the mesh generation, we first created a mapped two-dimensional mesh in the plane normal to the channel direction, and then mesh is swept along the channel direction (Fig. 4). The complete mesh consists of 19708 domain elements, 7392 boundary elements, and 972 edge elements.

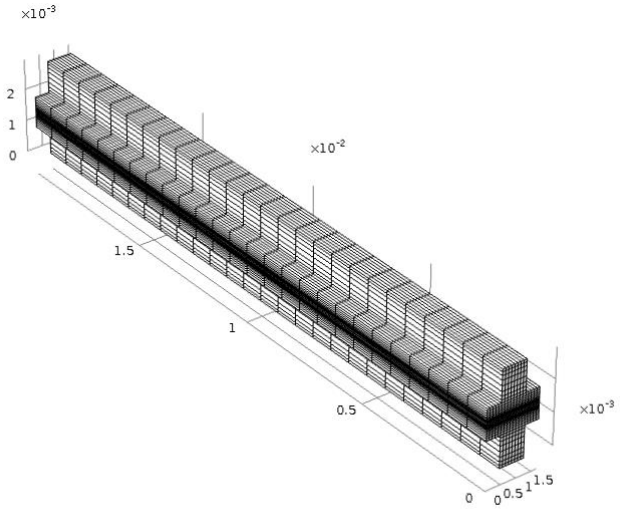

Figure 4. Mesh grid of solid acid fuel cell model.

2.1. Electrochemical currents

This modelling calculates parameters such as the cell voltage, the current density, and the gas composition of both anode and cathode of the fuel cell. When the equilibrium in the electrochemical reaction is established, the change in Gibbs free energy (G) pertaining to the electrochemical force is calculated using the following equation:

$$\Delta E = -\frac{\Delta G}{2F} = \frac{\Delta G^0}{2F} - \frac{RT}{2F}\ln(K) \quad (6)$$

The Nernst equation (Eq. 7) gives the open circuit cell potential (ΔE) as a function of cell temperature (T) and the reactant partial pressures (P_i).

$$\Delta E_{Nernst} = \Delta E_0 - 0.85\times10^{-3}(T-298.15) + \frac{RT}{2F}\ln\left(\frac{P_{H_2}\times P_{O_2}{}^{0.5}}{P_{H_2O}\times P^{0.5}}\right) \quad (7)$$

where ΔE_0 represents the reference potential at unity activity, R is the universal gas constant, P and F are the total pressure inside the stack and Faraday constant, respectively.

Electrochemical reactions taking place in the solid acid fuel cell generate the electricity current. Three classes of voltage drop, namely the activation (η_{act}), ohmic (η_{ohm}), and concentration (η_{conc}) over-voltages are responsible for reduction in output voltage. Thus, a holistic equation for the output voltage calculation can be written as:

$$V_{Cell} = \Delta E_{Nernst} - \eta_{act} - \eta_{ohm} - \eta_{conc} \quad (8)$$

Slowness of the individual chemical reactions performed at the two electrodes are the primary cause of activation losses (η_{act}), which are related to the energy barrier that the reactive species must overcome in order to sustain the reaction. The rate of current density upon the interface pertains to the activation over-potential proposed by the Butler-Volmer equations:

$$i_a = i_{0,a}^{ref}\left(\frac{C_{H_2}}{C_{H_2}^{ref}}\right)^{0.5}\left[\exp\frac{\alpha_a F}{RT}\eta_{act,a}) - \exp(-\frac{\alpha_c F}{RT}\eta_{act,a})\right] \quad (9)$$

where i_a is the current density in anode, i_0 represents the pre-exponential coefficient, α_a and α_c are so-called anodic and cathodic charge transfer coefficients and C is concentration. Tafel's equation offers activation drop in the cathode:

$$i_c = i_{0,c}^{ref}\left(\frac{C_{O_2}}{C_{O_2}^{ref}}\right)\times 10^{\frac{\eta_{act,c}}{A_c}} \quad (10)$$

where i_c is the current density in cathode and A_c is the so-called Tafel slope. The voltage drop related to the resistance to the electron flow in the electrodes and the resistance to the ionic flow in the electrolyte is denoted by ohmic losses (η_{ohm}). Ohm's law is used to calculate the associated potential loss as follows:

$$\eta_{ohm} = i\sum R_{ohm}^{o} = i\times(R_{elec}^{o} + R_{ionic}^{o}) \quad (11)$$

The value of the resistance (R^o) can be obtained theoretically, but for a rigorous determination it should be related to the operative conditions (e.g. temperature) and structure (thickness, materials, etc.) of each component of the cell, including both ionic and electronic mechanisms of conduction as:

$$R^{o} = \frac{t}{\sigma} \quad (12)$$

where t is thickness and σ is ionic or electric conductivity. Mass transfer resistance of the reacting species within the pores of the electrodes results in concentration loss. Reacting species have to diffuse through the pores of the electrodes to reach the sites where the electrochemical reaction takes place. The concentration voltage drop η_{conc} is expressed by:

$$\eta_{conc} = \frac{RT}{2F}\ln\left(1-\frac{i}{i_{Max}}\right) \quad (13)$$

The currents in solid acid fuel cells fall into two categories: ionic current and electronic current. Charge balance equations are solved to obtain solid phase and electrolyte phase potentials by using ohm's law:

$$\nabla.(\sigma_e^{eff}\nabla\varphi_e) = -S_\phi \quad (14)$$

$$\nabla.(\sigma_i^{eff}\nabla\varphi_i) = -S_\phi \quad (15)$$

where σ_e^{eff} is effective electronic conductivity of the solid phase, σ_i^{eff} is effective protonic conductivity of the membrane, φ_e and φ_i are solid phase and electrolyte phase potentials, respectively. We may set source term S_φ to zero in these domains since no reaction takes place in GDL and in the electrolyte. In anode and cathode catalyst layers, S_φ depends upon the local rate of reaction.

The kinetics driving force is the local surface over-potential, denoted as η_{an} and η_{cat} for the anode and cathode, respectively.

$$\eta_{an} = \phi_{sol} - \phi_{mem} \quad (16)$$

$$\eta_{cat} = \phi_{sol} - \phi_{mem} - \phi_{oc} \quad (17)$$

The subscripts of sol and mem denote the solid and membrane electrolyte. The gain in electrical potential from the anode to the cathode can be obtained by subtracting the open circuit voltage (φ_{oc}) calculated from the operating temperature [32]:

$$\phi_{oc} = 1.23 - 0.9\times10^{-3}(T-298) \quad (18)$$

2.2. Mass transfer

Diffusivity of species at varying operating temperature and pressure is given by [33,34]:

$$D_i = D_i^0(T_0,P_0)\left(\frac{P_0}{P}\right)\left(\frac{T}{T_0}\right)^{1.75} \quad (19)$$

The mechanism of diffusion in the porous environment of electrodes is different compared to gas channels because the average pore size was considerably smaller than the gas particle's mean free path. The diffusivities are corrected using the Bruggemann correction formula in order to account for geometric constraints of the porous media [35]:

$$D_{i,j}^{eff} = \varepsilon^{1.5} D_{i,j} \quad (20)$$

where ε is the value of porosity. The Maxwell-Stefan equation which describes diffusion in multicomponent systems is solved to determine parameters in the flow channels, GDLs and the porous electrode.

$$\nabla.(\omega_i \rho u - \rho \omega_i \sum_{j=1}^{k} D_{i,j}^{eff} (\frac{M}{M_j}(\nabla \omega_j + \omega_j \frac{\nabla M}{M}) + (x_j - \omega_j)\frac{\nabla P}{P})) = v_i \frac{iM_i}{n_i F} \quad (21)$$

where $D_{i,j}^{eff}$ is the effective multicomponent diffusivity of species i in j, u is flow velocity, M and $M_{i/j}$ are gas mixture and species i/j molecular mass, x and ω show molar and mass fractions, ν_i and n_i are stoichiometric coefficient and the number of electrons transferred in half reaction and ρ is the gas mixture density described by:

$$\rho = \frac{(\sum_i x_i M_i).p}{RT} \quad (22)$$

On the cathode side, two independent equations are solved for two species. The third species mass fraction is calculated upon using the mass balance equation provided as follows:

$$\omega_{N_2} = 1 - \omega_{O_2} - \omega_{H_2O} \quad (23)$$

On the anode side, the hydrogen mass fraction is obtained by solving the aforementioned equation and the mass fraction of water is calculated using the mass balance equation:

$$\omega_{H_2O} = 1 - \omega_{H_2} \quad (24)$$

2.3. Momentum transfer

The well-known continuity and Navier-Stokes equations are employed to model the flow profile in the gas channels:

$$\nabla.(\rho u) = 0 \quad (25)$$

$$\rho u.\nabla u = \nabla.[-PI + \mu(\nabla u + (\nabla u)^T)] \quad (26)$$

where μ denotes dynamic viscosity of the mixture and is calculated as:

$$\mu = \sum_i x_i \mu_i \quad (27)$$

Brinkman equation describes the flow through a porous media. Parameters are modeled by this equation in the porous gas diffusion layers and electrodes:

$$(\frac{\mu}{\kappa})u = \nabla.[-PI + (\frac{\mu}{\varepsilon})(\nabla u + (\nabla u)^T)] \quad (28)$$

Here, κ is permeability which is an intrinsic property of porous media. The continuity equation for the porous media becomes:

$$\nabla.(\rho \varepsilon u) = 0 \quad (29)$$

2.4. Boundary conditions

The anode GDL boundaries facing the flow pattern ribs are set to zero electronic potential, and the corresponding boundaries at the cathode side are set to the cell operating potential. All other external boundaries are electrically isolating.

At the flow channel inlet boundaries, laminar inlet flow velocity profiles are specified and gas velocity is calculated based on the stoichiometric ratio, fuel cell active area, and the flow channel dimensions are given as follows:

$$U_{in-cathode} = \lambda_c \frac{1}{4F} x_{O_2} \frac{RT}{PA_{channel} n_{channel}} \quad (30)$$

$$U_{in-anode} = \lambda_a \frac{1}{2F} x_{H_2} \frac{RT}{PA_{channel} n_{channel}} \quad (31)$$

where $U_{in\text{-}cathode}$ and $U_{in\text{-}anode}$ are the average inlet velocity on the cathode and anode sides, $A_{channel}$ is the channel cross-sectional area and

$n_{channel}$ is the channel number.

Outlet flow pressure is considered to be atmospheric pressure. The flow is assumed to be fully developed after a 10^{-3} meter entrance length. In order to model a multiple parallel channel configuration, symmetric boundary conditions are applied along the long sides of the GDLs and the porous electrodes. No-slip conditions are assumed in all other boundaries.

Mass fractions at the channel inlets are calculated and outflow conditions are used at the convective flux as shown below:

$$n.(-\nabla C_i) = 0 \tag{32}$$

At the GDL-electrolyte interface, the catalyst layer is assumed as an infinite thin layer, where the fluxes of each species are functions of the local current density described as follows:

$$N_{H_2} = -\frac{i_a}{2F} M_{H_2} \tag{33}$$

$$N_{O_2} = -\frac{i_c}{4F} M_{O_2} \tag{34}$$

$$N_{H_2O} = -\frac{i_c}{4F} M_{H_2O} \tag{35}$$

where N is the inward mass flux, i_a and i_c are local current densities at the anode side and cathode side. All other external boundaries are set to zero flux conditions.

The base case parameters used in the model are listed in Table 1.

Table 1
Model parameters.

Parameters	Value	Unit
Constants		
Gases universal constant	8.314	$j.mol^{-1}.K^{-1}$
Faraday constant	96500	$C.mol^{-1}$
Operating conditions		
Fuel cell temperature	250	$^{\circ}C$
Reference pressure	101325	Pa
Dynamic viscosity anode	1.201×10^{-5} (calculated)	Pa.s
Dynamic viscosity cathode	2.623×10^{-5} (calculated)	Pa.s
Mass fraction of H_2_anode	0.743 (calculated)	
Mass fraction of O_2_cathode	0.228 (calculated)	
Mass fraction of H_2O_cathode	0.023 (calculated)	
Anode reference voltage	0	V
Kinetic parameters		
Anodic and cathodic transfer coefficient for hydrogen oxidation reaction	$\alpha_a = \alpha_c = 1$	
Cathodic transfer coefficient for oxygen reduction reaction	$\alpha_c = 1$	
Reference hydrogen molar concentration	40.88	$mol.m^{-3}$
Reference oxygen molar concentration	40.88	$mol.m^{-3}$
Electrolyte properties		
Ionic conductivity	2 [36]	$S.m^{-1}$

Electrolyte thickness	50	μm
Catalyst layer information		
Catalyst layer thickness	25	μm
Anode exchange current density	10^5 [37]	$A.m^{-2}$
Cathode exchange current density	1 [37]	$A.m^{-2}$
GDL properties		
GDL thickness	380	μm
Electrical conductivity	222	$S.m^{-1}$
Porosity	0.4 [38]	
Permeability	1.18×10^{-11} [38]	m^2
Gas channel dimensions		
Length	2	cm
Cross section	0.7874×1	mm^2
Diffusion coefficient		
H_2-H_2O	1.949×10^{-4} (calculated)	$m^2.s^{-1}$
N_2-H_2O	5.452×10^{-5} (calculated)	$m^2.s^{-1}$
O_2-H_2O	5.974×10^{-5} (calculated)	$m^2.s^{-1}$
O_2-N_2	5.083×10^{-5} (calculated)	$m^2.s^{-1}$

3. Results and discussion

In the current work we have investigated the performance of the solid acid fuel cell using the presented model of the electrochemical reaction and transport phenomena, which are fully coupled with the governing equations. The equations were solved using the computational fluid dynamics (CFD) software, a finite elements technique solver from 0.4-0.95 V of cell potential by 0.05 step size.

The polarization curve, an indicator of the priority of fuel cell was used to compare the cell performance with a conventional cell. Simulation results were validated by generating polarization curves and comparing them with those presented by Chisholm et al. [36]. Grid independence tests were conducted to ensure that the simulations results are independent of the mesh size. For the three different mesh sizes, the difference between polarization curves is less than 1.0 % which ensures mesh size independence. In the first approach, complete mesh consists of 5772 domain elements, 3616 boundary elements, and 764 edge elements and 44552 degrees of freedom are considered. The second approach consists of 19708 domain elements, 7392 boundary elements, and 972 edge elements and 146045 degrees of freedom. Similarly, for the third approach, complete mesh consists of 42228 domain elements, 15528 boundary elements, and 1564 edge elements and 315746 degrees of freedom.

The current-voltage curve of the model is shown in Fig. 5. We can clearly observe the good agreement between the model and the experimental data. However, early deviation lies within a region which is not a conventional operating range of fuel cells. At low current densities, the concentration of hydrogen is high and a decline in voltage of the cell is mainly due to mass transfer limitation of hydrogen.

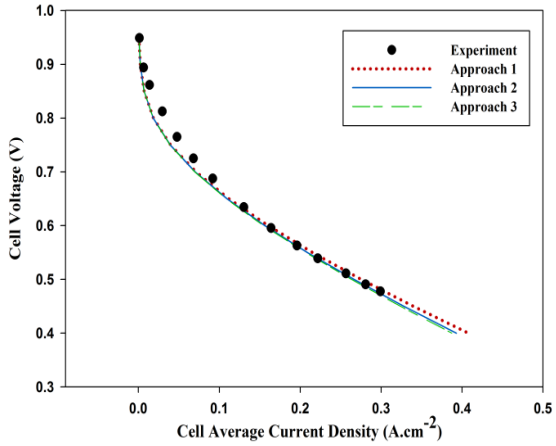

Figure 5. Polarization curve.

The power density curve generated by the simulation is shown in Fig. 6. The relation between voltage, current density and the power of the fuel cell is P =V.I. It is clear that maximum cell power (1612.19 $W.m^{-2}$) was observed at medium current densities (namely 0.46 $A.cm^{-2}$) which suggests the optimum range of fuel cell operation.

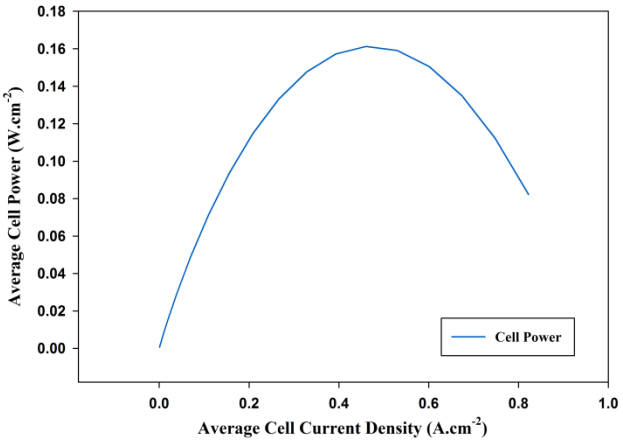

Figure 6. Power density curve.

Concentration of reactants is an important factor in the reaction rate and electric current. The concentration gradient between electrodes and the channels leads to diffusion of species into the porous electrodes. Figure 7 shows hydrogen mass fraction at the anode side. The mass fraction of H_2 decreases along the flow direction. In the cross-sectional view, the mass fraction of H_2 is higher in the channel and lower in the porous GDL, where diffusion dominates the species mass transport in the porous media.

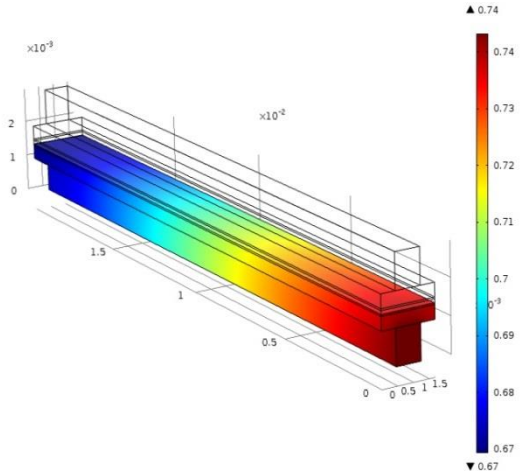

Figure 7. Hydrogen mass fraction distribution in anode side.

Illustration of the oxygen concentration profile within the air channel and the cathode is given in Fig. 8. It demonstrates that by going along the channel, the amount of oxygen decreases due to consumption in reaction. Furthermore, in the cross-sectional view, the decrease in mass fraction of hydrogen in the anode side is less than oxygen in the cathode side due to the lower diffusivity coefficient of oxygen and water formation which blocks the porous area in the cathode side.

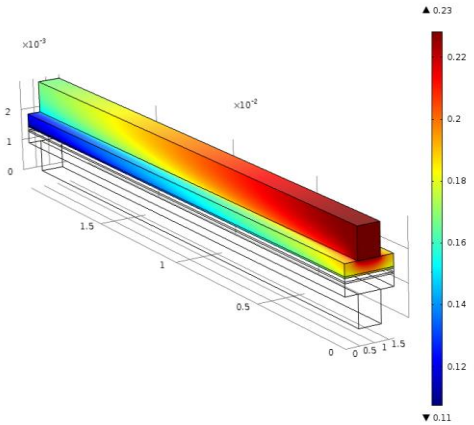

Figure 8. Oxygen mass fraction distribution in cathode side.

Figure 9 shows the ionic current in the cell length direction at the center of the electrolyte. Local current density decreases along the channels due to reduction of the reactants concentration. In the wide direction, the currents density is highest in the region close to the channel, where the reactant concentrations are higher.

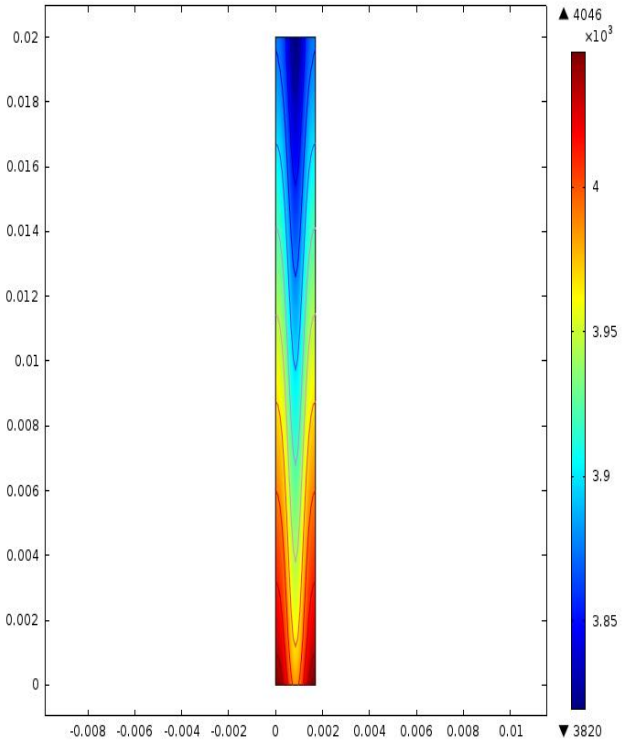

Figure 9. Ionic current in the cell length direction at the center of the electrolyte.

Water management plays an important role on performance of the cells. Variation in water causes dehydration or flooding which must be controlled during working of the fuel cell. Figure 10 shows the mass fraction of water on the anode side. On the anode side, because there is no osmotic drag effect on the CsH_2PO_4 electrolyte, there is no water transfer from the anode to the cathode as the proton moves that way. As a result, the anode water mass fraction increases slightly due to the consumption of hydrogen.

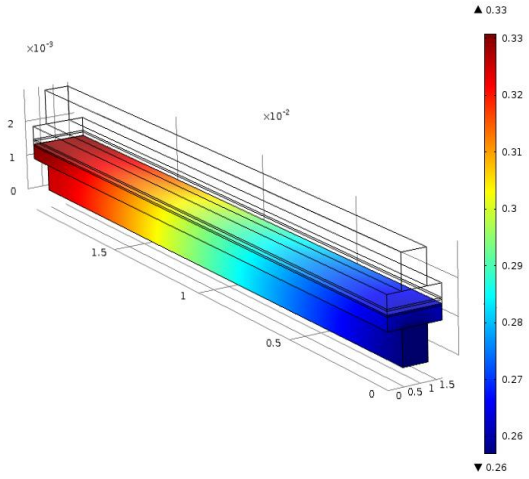

Figure 10. Water mass fraction distribution in anode side.

Due to high temperature inside the cell, water produced by reaction is in vapor phase. Figure 11 shows the water distribution in the cathode side. As shown, water mass fraction increases along the channel due to the water production by oxygen consumption at the catalyst layer. As water is produced on the cathode catalyst layer, it has a high molar fraction at the cathode GDL near the catalyst.

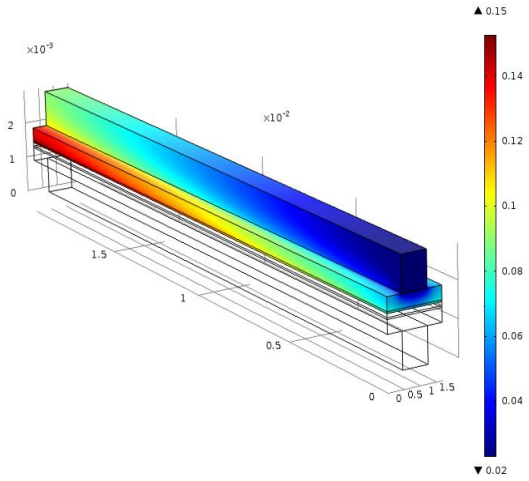

Figure 11. Water mass fraction distribution in cathode side.

All results are provided for 0.4V operating voltage. In Fig. 12, it is evident that at lower voltages, the difference between predicted and current densities increases. This is

because at higher current densities, the rate of reaction is faster as compared to transport of the reactants, and thus concentration losses in the polarization curve are dominant.

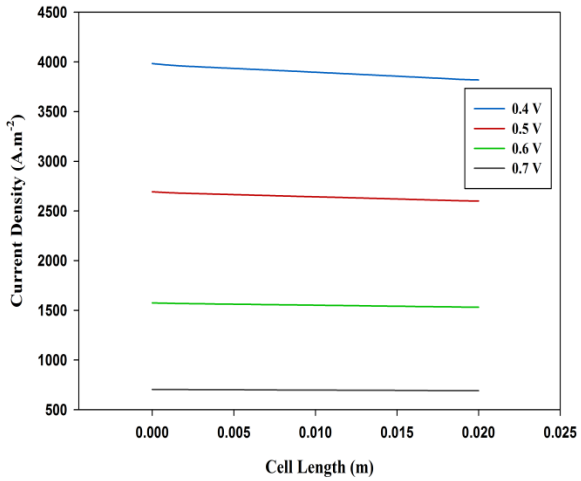

Figure 12. Current density curves for different voltages.

As it is shown in Fig. 13, the amount of hydrogen decreases, especially at lower voltage by moving along the channel. Strong reduction of hydrogen is sensed due to higher current density and consequently higher consumption of species. It must also be mentioned that at a high voltage, oxygen consumption is less than low voltage which is obvious in Fig. 14.

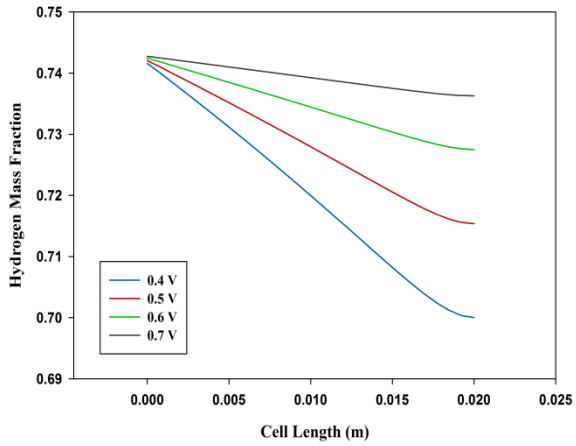

Figure 13. Hydrogen mass fraction curves for different voltages.

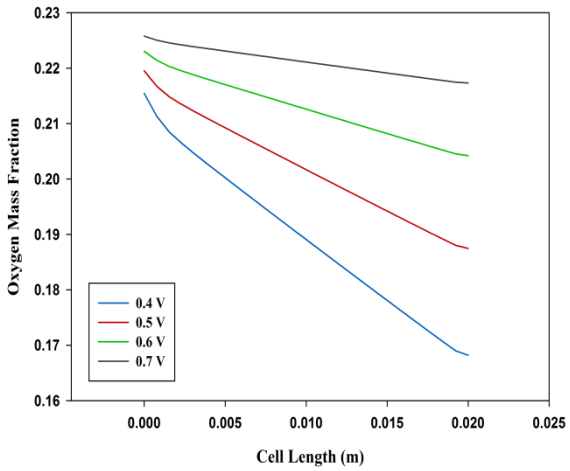

Figure 14. Oxygen mass fraction curves for different voltages.

Figure 15 shows that higher consumption of hydrogen leads to an increase in water mass fraction in the anode side at lower voltages. Also, the mass fraction of water at the cathode side is shown in Fig. 16 which also shows higher production of water at lower voltage. This is because the rate of liquid water production is higher due to higher current density. As the current density further increases, electro osmotic drag also increases. However, large amounts of water are produced in the cell.

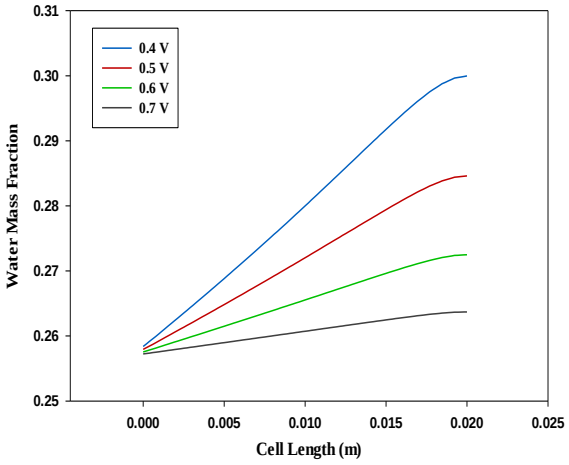

Figure 15. Water mass fraction curves for different voltages in anode side.

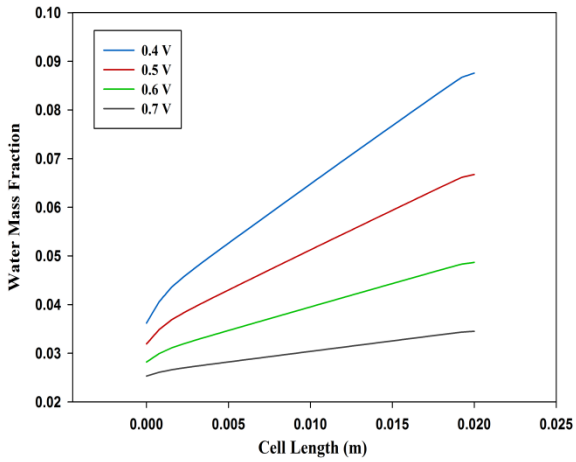

Figure 16. Water mass fraction curves for different voltages in cathode side.

4. Conclusions

In this study, a three-dimensional computational fluid dynamics model of solid acid fuel cell was developed to predict cell performance and investigate the effect of cell parameters. The simulated model was based on solving the equations for flow channel, GDLs, catalyst layers and electrolyte which is discretized on the base of the finite elements method. This study presents the following conclusions: The need to humidify is not required as proton conductivity in the solid acids electrolyte such as CsH_2PO_4 depends on conduction of protons through the solid matrix. H_2/O_2 fuel cells were successfully run with CsH_2PO_4 electrolyte. The successful use of CsH_2PO_4 in fuel cell applications in this study represents a confirmation of the feasibility of CsH_2PO_4 as a proton conducting electrolyte in real applications.

Nomenclature

C	molar concentration [$mol.m^{-3}$].
D	mass diffusion coefficient [$m^2.s^{-1}$].
E	cell potential [V].
F	Faraday constant [coulomb/mol].
i	local current density [$A.m^{-2}$].
M	molar mass [$Kg.mol^{-1}$].
P	pressure [Pa].
t	thickness [m].
T	temperature [K].
U	velocity vector [$m.s^{-1}$].
x	mole fraction.

Greek symbols

ω	mass fraction.
μ	viscosity [Pa.s].
Φ	potential [V].
ρ	density of the mixture [$Kg.m^{-3}$].
σ	conductivity [$S.m^{-1}$].
α	transfer coefficient.
η	over-potential [V].
ε	porosity.
κ	permeability [m^2].

Subscripts and superscripts

a, an	anode.
act	activation.
c, cat	cathode.
conc	concentration.
eff	effective.
elec, e	electronic.
max	maximum.
mem	membrane.
ohm	ohmic.
ref	reference condition.
sol	solid.

References

[1] Dupuis, A. C., "Proton exchange membranes for fuel cells operated at medium temperatures: Materials and experimental techniques", *Prog. Mater. Sci.*, **56** (3), 289 (2011).

[2] Demirbas, A., "Fuel cells as clean energy converters", *Energy Sources*, **29** (2), 185 (2007).

[3] McLellan, B., Costa, D., Dicks, A., Rudolph, V., Pagan, R., Sheng, C. and Wall, T., "Hydrogen economy options for Australia", *Dev. Chem. Eng. Miner. Process*, **12** (5), 447 (2004).

[4] Uda, T., Boysen, D., Chisholm, C. and Haile, S., "Alcohol fuel cells at optimal temperatures", *Electrochem. Solid-State*

Lett., **9** (6), 261 (2006).

[5] Muis, Z., Hashim, H., Manan, Z. and Douglas, P., "Effects of fossil fuel price fluctuations on electricity planning comprising renewable energy", *Asia-Pac. J. Chem. Eng.*, **6** (3), 552 (2011).

[6] Uda, T. and Haile, S., "Thin-membrane solid acid fuel cell", *Electrochem. Solid-State Lett.*, **8** (5), 245 (2005).

[7] Ahn, Y., Mangani, I., Park, C. and Kim, J., "Study on the morphology of CsH_2PO_4 using the mixture of methanol and polyols", *J. Power Sources*, **163** (1), 107 (2006).

[8] Yoshimi, S., Matsui, T., Kikuchi, R. and Eguchi, K., "Temperature and humidity dependence of the electrode polarization in intermediate-temperature fuel cells employing CsH_2PO_4/SiP_2O_7-based composite electrolytes", *J. Power Sources*, **179** (2), 497 (2008).

[9] Haile, S., Boysen, D., Chisholm, C. and Merle, R., "Solid acids as fuel cell electrolytes", *Nature*, **410** (6831), 910 (2001).

[10] Yamane, Y., Yamada, K. and Inoue, K., "Superprotonic solid solutions between $CsHSO_4$ and CsH_2PO_4", *Solid State Ionics*, **179** (13), 483 (2008).

[11] Ponomareva, V., Kovalenko, K., Chupakhin, A., Shutova and E., Fedin, V., "$CsHSO_4$-Proton conduction in a crystalline metal-organic framework", *Solid State Ionics*, **225**, 420 (2012).

[12] Lavrova, G., Russkih, M., Ponomareva, V. and Uvarov, N., "Intermediate-temperature fuel cell based on the proton conducting composite membranes", *Solid State Ionics*, **177** (19), 2129 (2006).

[13] Ortiz, E., Vargas, R. and Mellander, B., "Phase behaviour of the solid proton conductor $CsHSO_4$", *J. Phys.: Condens. Matter*, **18** (42),9561 (2006).

[14] Merinov, B., "Proton transport mechanism and pathways in the superprotonic phase of $CsHSO_4$ from experiment and theory", *Solid State Ionics*, **213**, 72 (2012).

[15] Chisholm, C. and Haile, S., "Entropy evaluation of the superprotonic phase of $CsHSO_4$: Pauling's ice rules adjusted for systems containing disordered hydrogen-bonded tetrahedral", *Chem. Mater.*, **19** (2), 270 (2007).

[16] Boysen, D., Haile, S., Liu, H. and Secco, R., "Conductivity of potassium and rubidium dihydrogen phosphates at high temperature and pressure", *Chem. Mater.*, **16** (4), 693 (2004).

[17] Otomo, J., Minagawa, N., Wen, C., Eguchi, K. and Takahashi, H., "Protonic conduction of CsH_2PO_4 and its composite with silica in dry and humid atmospheres", *Solid State Ionics*, **156** (3), 357 (2003).

[18] Taninouchi, Y., Uda, T. and Awakura, Y., "Dehydration of CsH_2PO_4 at temperatures higher than 260 °C and the ionic conductivity of liquid product", *Solid State Ionics*, **178** (31), 1648 (2008).

[19] Boysen, D., Uda, T., Chisholm, C. and Haile, S., "High-performance solid acid fuel cells through humidity stabilization", *Science*, **303** (5654), 68 (2004).

[20] Hayashi, S. and Mizuno, M., "Proton diffusion in the superprotonic phase of $CsHSO_4$ studied by ^1H NMR relaxation", *Solid State Ionics*, **171** (3), 289 (2004).

[21] Hogarth, W., Costa, D. and Lu, G., "Solid acid membranes for high

temperature (>140 ˚C) proton exchange membrane fuel cells", *J. Power Sources*, **142** (1), 223 (2005).

[22] Compton, M., Maynes, K., Pavelites, J. and Baker, D., "Proton NMR relaxation study of the $CsHSO_4$ solid acid system", *Solid State Commun.*, **136** (3), 138 (2005).

[23] Yang, C., Costamagna, P., Srinivasan, S., Benziger, J. and Bocarsly, A., "Approaches and technical challenges to high temperature operation of proton exchange membrane fuel cells", *J. Power Sources*, **103** (1), 1 (2001).

[24] Boysen, D., Uda, T., Chisholm, C., Haile, S., "High-performance solid acid fuel cells through humidity stabilization", *Science*, **303** (5654), 68 (2004).

[25] Otomo, J., Tamaki, T., Nishida, S., Wang, S., Ogura, M., Kobayashi, T., Wen, C., Nagamoto, H. and Takahashi, H., "Effect of water vapor on proton conduction of cesium dihydrogen phosphate and application to intermediate temperature fuel cells", *J. Appl. Electrochem.*, **35** (9), 865 (2005).

[26] Haile, S., Chisholm, C., Sasaki, K., Boysen, D. and Uda, T., "Solid acid proton conductors: From laboratory curiosities to fuel cell electrolytes", *Faraday Discuss.*, **134**, 17 (2007).

[27] Ponomareva, V. and Shutova, E., "High-temperature behavior of CsH_2PO_4 and CsH_2PO_4–SiO_2 composites", *Solid State Ionics*, **178** (7), 729 (2007).

[28] Xie, Q., Li, Y., Hu, J., Chen, X. and Li, H., "A CsH_2PO_4-based composite electrolyte membrane for intermediate temperature fuel cells", *J. Membr. Sci.*, **489**, 98 (2015).

[29] Qing, G., Kikuchi, R., Takagaki, A., Sugawara, T. and Oyama, S., "CsH_2PO_4/Epoxy Composite Electrolytes for intermediate temperature fuel cells", *Electrochim. Acta*, **169**, 219 (2015).

[30] Bessette, N. and Wepfer, W., "Electrochemical and thermal simulation of a solid oxide fuel cell", *Chem. Eng. Commun.*, **147** (1), 1 (1996).

[31] Park, J. and Min, K., "Dynamic modeling of a high temperature proton exchange membrane fuel cell with a fuel processor", *Int. J. Hydrogen Energy*, **39** (20), 10683 (2014).

[32] Meng, H., "Numerical studies of liquid water behaviors in PEM fuel cell cathode considering transport across different porous layers", *Int. J. Hydrogen Energy*, **35** (11), 5569 (2010).

[33] Guvelioglu, G. and Stenger, H., "Computational fluid dynamics modeling of polymer electrolyte membrane fuel cells", *J. Power Sources*, **147** (1), 95 (2005).

[34] Bird, R., Stewart, W. and Lightfoot, E., Transport phenomena, Wiley, New York, (1960).

[35] Bear, J. and Buchlin, J., Modelling and applications of transport phenomena in porous media, Kluwer Academic Publishers, Dordrecht The Netherlands, (1991).

[36] Chisholm, C., Boysen, D., Papandrew, A., Zecevic, S., Cha, S., Sasaki, K., Varga, A., Giapis, K. and Haile, S., "From laboratory breakthrough to technological realization: The development path for solid acid fuel cells", *Interface*, **18** (3), 53 (2009).

[37] Cheddie, D. and Munroe, N., "Three dimensional modeling of high temperature PEM fuel cells", *J. Power*

Sources, **160** (1), 215 (2006).

[38] Broka, K., Characterization of the components of the proton exchange membrane, Ph.D. dissertation, Royal Institute of Technology, Stockholm, (1995).